RESEARCH ARTICLE

Macromolecular Materials and Engineering
Open Access
www.mame-journal.de

Infill Density Effects on the Mechanical and Thermal Properties of Copper-Plated 3D Printed Parts

Tommaso Ludergnani, Giulia Fredi, Lorenzo Malagutti, Andrea Balbo, Andrea Dorigato, Francesco Mollica, and Valentina Mazzanti*

Fused Filament Fabrication (FFF) is a 3D-printing technique that enables the production of complex geometries with a high level of customization at low cost. The poor mechanical properties of FFF-printed parts often undermine the application of this technology for structural purposes. To overcome this limitation, a two-step metallization method is performed to deposit a copper layer on the exterior of an Acrylonitrile–Butadiene–Styrene (ABS) substrate, using a non-toxic and cost-effective plating solution. Electroplating over the exposed grid infill, at various densities, is exploited to improve the load transfer between copper and ABS. The resulting samples are characterized mechanically and thermally, and finite element modeling simulations are used to better understand the characterization results. It is found that an infill of 50–60% provides the best compromise between mechanical performance and thermal conductivity because the infill density is low enough to allow copper penetration into the material to create a strong mechanical interlocking with ABS, yet high enough to create multiple conductive bridges through the thickness of the sample. This study demonstrates the effectiveness of electroplating as a post-processing technique to simultaneously enhance the mechanical and thermal properties of FFF-printed parts and provides insights into the optimal design parameters for achieving this goal.

1. Introduction

Fused Filament Fabrication (FFF), also known as "Fused Deposition Modeling", is one of the most common additive manufacturing technologies based on material extrusion that is used in 3D printing of thermoplastics.[1,2] The polymeric material, usually in the form of a filament, is pushed through a heated nozzle where it melts and is subsequently extruded upon a heated bed following a predetermined path that is set through the planar motion of the extruder holding the nozzle. Objects are then created by successive layer depositions. One of its main advantages is that it allows the fabrication of parts of rather complex shapes with low investment costs, without large quantities of scrap, and in a simpler way compared to the more traditional forming techniques.[3,4] On the other hand, parts manufactured via FFF have some well-known problematic issues, the main one being the lengthy manufacturing procedure, but noteworthy also are the inferior surface aesthetic quality[5–7] and the lower mechanical properties.[7–12]

Surface quality improvements can be achieved by electroplating with a suitable metal coating (e.g., copper or nickel): plastics are often coated with metals to improve the aesthetic appearance and to increase thermal and electrical conductivity[13]. A thin metallic layer is deposited through an electrochemical process in a plating solution, in which metal cations are reduced on the polymeric surface by a continuous electrical charge. This procedure is very common in the automotive and electronic industries and is known as metallization.[14,15]

A necessary requirement for electroplating is that the substrate be electrically conductive, therefore since plastics are typically insulating materials, a pre-treatment known as "primary metallization" is first implemented to induce electrical conductivity. The actual metal plating is performed next as a subsequent step.[16]

Primary metallization can be performed in many ways. Some literature studies present an electroless plating method, which is effective and enables an adequate interface between the polymer substrate and the metal layer.[6,17–19] On the other hand, this method is complex, generally expensive, is performed at higher temperatures, and makes use of substances that are dangerous for the environment (e.g., chromium), or it requires expensive

T. Ludergnani, L. Malagutti, F. Mollica, V. Mazzanti
Department of Engineering
University of Ferrara
Via Saragat 1, Ferrara 44122, Italy
E-mail: francesco.mollica@unife.it
G. Fredi, A. Dorigato
Department of Industrial Engineering
University of Trento
Via Sommarive 9, Trento 38123, Italy
A. Balbo
Corrosion and Metallurgy Study Centre "A. Daccò"
University of Ferrara
Ferrara 44121, Italy

The ORCID identification number(s) for the author(s) of this article can be found under https://doi.org/10.1002/mame.202300203

DOI: 10.1002/mame.202300203

Figure 1. Schematic phases of the process.

materials such as palladium.[20,21] For these reasons, other researchers have explored different alternatives, such as surface treatments using a conductive paste,[15] a metallic paint,[16,21,22] or graphite powder.[23,24] In all these techniques the conductive substance is placed directly upon the surface of the plastic sample, thus leading to a simpler procedure and in some cases to a reduction in the environmental impact.

Many scientific articles dealing with electroplated FFF-printed parts aim at reducing surface roughness,[5,18,23,24] or are concerned with dimensional variations after plating[5] and the quality of the layer adhesion between the polymer and the metal coating.[21] From the standpoint of industrial applications, a relevant interest is the production of electrically active parts, such as electric discharge machining electrodes[19,22,25] or solenoid inductors.[26] Based on the authors' knowledge, however, there are no studies in the scientific literature about using electroplating on an FFF-printed substrate to improve the mechanical properties, provided that the electrodeposited layer is sufficiently thick. Indeed, this is very interesting, since the deposition of metal on the outer surface leads to higher flexural properties, as the stiffest and strongest material would be located far from the neutral axis.

For this goal, a high-quality interface between the metal coating and the polymeric substrate is an important requirement. As the two materials are generally incompatible and the chemical etching that is typical of electroless plating is not considered here, the only solution is to exploit the controllable surface roughness of 3D printed parts to promote mechanical interlocking between metal and plastics, thereby improving adhesion. FFF, in fact, allows to adjust the printing parameters to conveniently control the surface geometry of the part. Moreover, if the printed part is left without the top and bottom layers, the exposed infill (i.e., the structure and amount of material used in the interior of the printed part) would function as an open superficial porosity, traversing the whole printed object. This can be partly filled by the deposited metal layer, thereby creating a stronger mechanical bond and the optimization of this process is the aim of the present article.

In this work, an eco-sustainable metallization is achieved through a two-step plating process that is free from chromium and precious metals. The pre-treatment is performed by treating an Acrylonitrile–Butadiene–Styrene (ABS) substrate with a pyrrole solution that is subsequently polymerized to form polypyrrole (PPy) prior to copper electroplating, following the method described in Ref. [20]. The effect of the infill density percentage on the mechanical properties of FFF-printed specimens made of ABS plated with copper is studied through flexural characterization. Interestingly, copper plating would also influence the thermal properties, and these are explored through light flash analysis.

Table 1. Printing parameters.

Parameters	Values	Parameters	Values
Layer height [mm]	0.25	Bed temperature [°C]	105
Line width [mm]	0.4	Infill density [%]	30–100
Nozzle diameter [mm]	0.4	Printing speed [mm s^{-1}]	15
Nozzle temperature [°C]	247	Contour lines	0

2. Experimental Section

2.1. Materials

A commercial ABS filament with a nominal diameter of 1.75 mm was purchased from Sunlu (Guangdong, China). Pyrrole (>98% FCC, FG), $CuSO_4 \cdot 5H_2O$, and $FeCl_3$ were obtained from Sigma–Aldrich (St. Louis, MO, USA). Pure copper anodes (99%) in the form of 100 mm × 50 mm plates and a thickness of 5 mm, were purchased from Admetal (Chwaszczyno, Poland).

2.2. Sample Preparation

The procedure is schematized in **Figure 1**. Before printing, the filament was dried at 80 °C for 24 h, and the reel was stored in silica gel during the printing process. All samples were drawn with freeCAD, saved in STL format, further processed with the Cura Slicer for setting all the printing parameters, and then printed with a desktop printer model i3 Mega S by Anycubic (Shenzhen, China). All relevant printing parameters are listed in **Table 1**. Some samples having a 100% infill density were used for the electrical characterization, to verify the effectiveness of primary metallization, while the specimens for mechanical and thermal characterization were printed with infill densities of 30%, 40%, 50%, 60%, 70%, and 100%. A ± 45° grid infill pattern was chosen, and all samples were printed without the top and bottom external surfaces.

After printing, ABS parts were made electrically conductive using a PPy treatment, with a procedure similar to that outlined in Refs. [20, 27]. All specimens were immersed in a 0.6 M aqueous solution of pyrrole (Py) for 10 min at room temperature, then a 0.9 M solution of $FeCl_3$ was slowly added dropwise under stirring, to induce Py polymerization on the ABS surface. After 30 min the samples were rinsed in distilled water and ethanol. Next, all incoherent PPy on the ABS surface was brushed away, and the whole procedure was repeated once more.

Finally, electroplating with copper was performed in two electrode cells as follows: the PPy-treated samples were immersed in an aqueous solution of $CuSO_4 \cdot 5H_2O$ (215 g L^{-1}) and H_2SO_4 (60 g L^{-1}) at room temperature and cathodically polarized, using copper plates as anodes. Filtered compressed air was pumped

into the bath to agitate the solution, in order to obtain a uniform plating thickness. Electrodeposition was carried out with an EG&G 273 potentiostat/galvanostat (Princeton Applied Research, Boston MA, USA) in galvanostatic mode. A current density of 10 mA cm^{-2} was used in the plating process, except for the first 10 min, during which it was set to 1 mA cm^{-2} to obtain a more uniformly plated surface.

The specimens having 100% infill density were plated for ≈48 min, which on the basis of Faraday's law and specimen geometry should have resulted in a nominal thickness of 100 µm. The specimens having a lower infill density were plated in such a way that the apparent density of the final plated specimen was ≈3 g cm^{-3}, and the plating times were achieved by trial and error. The mass and dimensions of each sample were measured before and after plating using an analytical balance (Mettler AE240, 0.01 mg resolution, Columbus OH, USA) and a digital micrometer (Mitutoyo 293, 1 µm resolution, Kawasaki, Japan), respectively.

2.3. Morphology of the 3D Samples

The morphology of uncoated ABS, PPy-coated ABS, and copper-plated specimens was investigated by optical microscopy and scanning electronic microscopy (SEM), using the Leica Microsystem CH-9435 (Wetzlar, Germany) and the ZEISS EVO MA 15 (Oberkochen, Germany) coupled with an energy dispersive detector (X-Max50 by Oxford Instruments, Abingdon, UK), respectively. In addition, optical observations were performed on the cross-section of the plated specimens to evaluate the copper layer thickness and the penetration depth as a function of the infill percentage.

2.4. Testing Procedures

Mechanical properties were measured through three-point bending tests according to the ISO 178 standard, which were performed at room temperature with an INSTRON 4467 dynamometer (Norwood, MA, USA) equipped with a 500 N load cell. The distance between the supports was 70 mm and the crossbar speed was 1 mm min^{-1}. Three samples of uncoated and copper-plated ABS for each geometry (dimensions 120 mm × 10 mm × 4 mm) were tested. The average values of the relevant mechanical parameters and their standard deviations were acquired by a LabVIEW-based self-developed software (National Instruments, Austin, TX, USA). According to the standard, the maximum flexural stress σ_f was calculated as:

$$\sigma_f = \frac{3FL}{2bd^2} \tag{1}$$

where F is the applied load, L is the distance between the supports, b is the width and d is the thickness of the specimen, while the maximum flexural strain ϵ_f was given by:

$$\varepsilon_f = \frac{6\delta d}{L^2} \tag{2}$$

where δ is the measured displacement. As a result, the Young's modulus in bending, E_f, can be obtained as follows:

$$E_f = \frac{1}{4}\,\frac{L^3}{bd^3}\,\frac{F}{\delta} \tag{3}$$

from which it is evident that the Young's modulus is proportional to the slope of the load–displacement curve. It is worth remarking that Equations (1)–(3) hold only in the case of uniform cross-section. For instance, they are not valid in the case of copper plated specimens, which are more similar to sandwich structures.

The thermal diffusivity of the samples was measured with a light flash analyzer LFA 467 (Netzsch Holding, Selb, Germany). To maximize the surface absorption and emissivity, both sides of the specimens were coated with a graphite spray, as recommended by the instrument producer. The test was performed at 25 °C on three samples for each infill percentage, and five pulses were performed per specimen. The samples were shaped as disks of 12.7 mm nominal diameter and 2 mm of thickness. Data were fitted via the Proteus software v. 8.0.3 (Netzsch) by applying the penetration model and a numerical pulse correction. The external copper layer was grounded away from the lateral surface of the specimens, to avoid any lateral preferential paths for heat conduction.

Electrical resistivity was measured in a four-point configuration following the ASTM D4496-04 standard. The tests were carried out on rectangular 3D printed specimens with nominal dimensions 5 mm × 20 mm × 3 mm. A DC voltage generator ISO-Tech IPS 303DD (Milano, Italy) was connected to the specimen, an ammeter was connected in series to measure the current flowing in the specimen, and a voltmeter was connected to the two inner electrodes to measure the voltage drop between them. The electrical resistivity ρ was determined at input voltages ranging from 0.5 to 8 V as, $\rho = R/(A\,t)$, where R is the electrical resistance calculated as the ratio between the measured voltage drop and the measured current, A is the cross-sectional area of the specimen, and t is the distance between the two inner electrodes, equal to 3.69 mm.

Electrical resistivity measurements were performed only to verify the effectiveness of the PPy treatment. The mean and standard deviation values obtained were 48 ± 12 Ω cm, which could be considered suitable for electroplating.[26]

2.5. Finite Element Modeling

The three-point bending tests of copper-plated specimens were also simulated using the finite element method (FEM) through the commercial software ANSYS 2021R1 (Canonsburg, PA, USA). The primary goal of these simulations was not to reproduce the experimental testing but rather to understand whether the interfacial adhesion between the base polymer and the metal coating was of good quality or not. To this aim, one must consider that in the FEM simulations, an ideal polymer-metal interface was assumed, as it was common in these cases. The PPy layer was not considered in the simulations, due to its extreme thinness, therefore PPy coated ABS was assumed to be a single material. Plated specimens were treated as sandwich structures, the PPy-treated ABS interior representing the core, while the copper

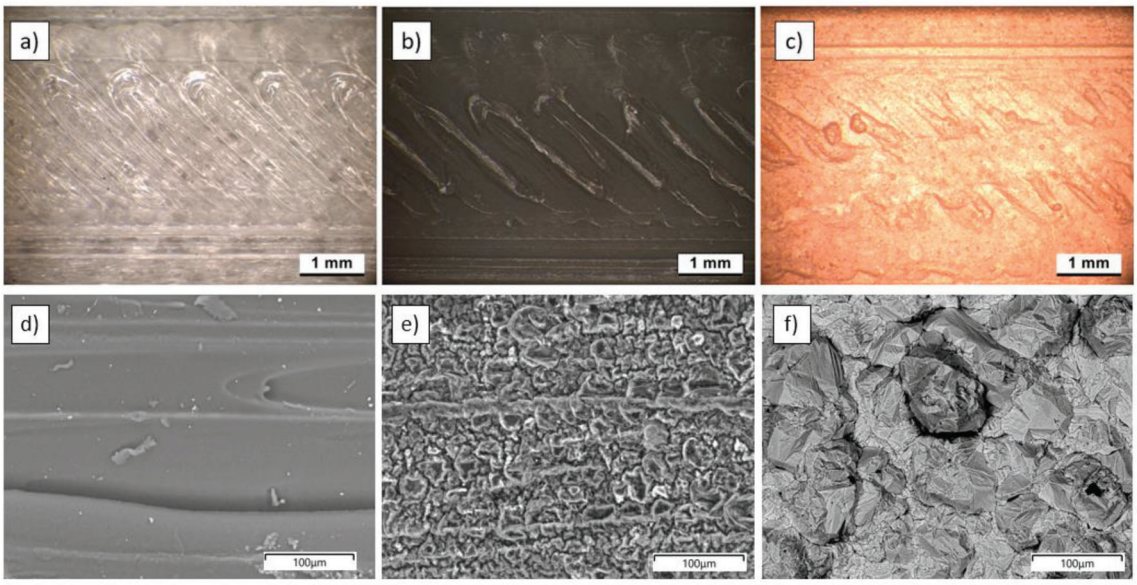

Figure 2. Surface morphology of a) ABS, b) ABS treated with PPy, and c) copper-plated specimens obtained by optical microscopy and d) uncoated ABS, e) ABS coated with PPy, and f) copper-plated specimens obtained by SEM. All samples that are shown had 100% infill density.

plating were the face sheets. In the simulation of the three-point bending tests, since the lateral ends of the specimen were simply supported, the vertical displacements were set equal to zero at both supports, while the horizontal displacement was set to zero at one of the two supports to avoid free-body motion. External loading was applied by superimposing the displacement of the mid-section of the specimen, i.e., at half its length. The applied force was then evaluated by considering the reaction force at the mid-section.

All materials were assumed as isotropic and linearly elastic until yielding, while the post-yield behavior was modeled using an isotropic hardening rule. The polymeric interior was modeled like a homogeneous material using 8-node SOLID185 brick elements. This had the effect of neglecting the precise architecture of the grid infill, which was a reasonable assumption in this case. The mechanical properties were then measured experimentally as averaged quantities, and they will be listed in the next section, since they are part of the results.

The copper plating was modeled as thin plates that were perfectly adherent to the ABS core, and 4-node SHELL181 elements attached to the brick elements were used. Since copper was deposited by a reduction reaction directly on the ABS substrate, it was assumed to be in its unalloyed state, thus displaying an elastoplastic mechanical behavior with a Young's modulus of 117 GPa, a Poisson's ratio of 0.34, a yield stress of 200 MPa, and a yield hardening slope of 10 GPa. These data were found to fit properly the stress versus strain curve of pure copper[28] and the "direct current plated copper" that was studied in Ref. [29].

3. Results and Discussion

3.1. Morphological and Mechanical Properties

Figure 2a–c shows the surface morphologies as obtained by optical microscopy for all 100% infill density specimens, i.e., for untreated, PPy-treated, and copper-plated materials, respectively. The modifications induced by the surface treatments are clearly visible. The PPy-treated surface (Figure 2b) is black and uniform, suggesting that the PPy covers the specimen surface in a very homogeneous way. The copper-plated surface (Figure 2c) appears to be regular and compact, although the surface texture conferred by the 3D printing process is partly revealed through the copper layer.

In Figure 2d–f, the corresponding SEM images are displayed. The untreated PLA surface is quite smooth, and the thin beads deposited by the extruder can be seen on the external surface. In fact, the material is dragged during the 3D printing process and stretched along the extrusion direction. By comparing Figure 2d,e, it can be seen that PPy treatment results in a surface roughness increase, as also found in Ref. [20]. Lastly, Figure 2f shows that the copper-plated surface is characterized by a globular structure,[20] despite appearing smooth at the lower magnifications.

Figure 3 shows the cross-section of the copper-plated ABS with a 100% infill density. As the whole cross section is dark, it can be concluded that the PPy treatment was able to reach also the inner portion of the sample. Indeed, since in the PPy treatment, the samples were soaked in pyrrole for a relatively long time, it can be assumed that pyrrole was able to diffuse into the ABS, thus leading to the dark coloring of the cross-section. As a further consequence, one may assume that PPy has a strong adhesion to the ABS surface, possibly as a result of pyrrole adsorption. The same cannot be said about the copper layer, which can be clearly distinguished from the PPy-treated ABS substrate. Nevertheless, copper covers the surface of the sample uniformly without macroscopic defects such as porosity or inclusions. The copper layer is ≈100 µm thick, and this thickness value is a compromise between the sought increase in the flexural mechanical properties and a relatively small weight increase. Since the specimens are ≈4 mm thick, copper plating covers ≈5% of the total thickness.

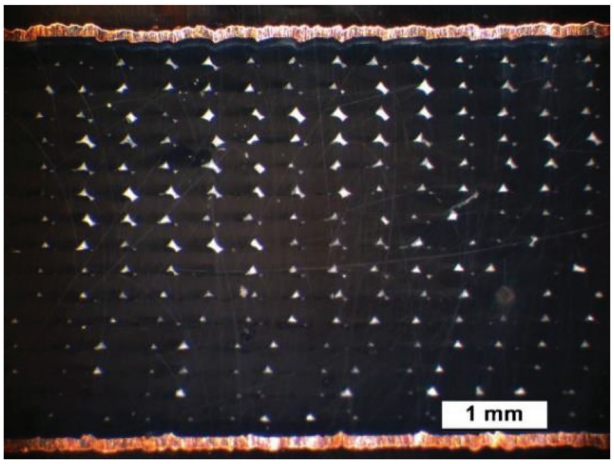

Figure 3. Cross section of a 100% infill copper-plated specimen.

Figure 4 shows representative stress versus strain curves in bending for neat ABS, PPy-treated ABS, and copper-plated ABS, all printed with 100% infill density. In the case of copper-plated ABS, stress and strain are to be intended as apparent quantities, because the specimens are obviously not homogeneous.

The flexural properties of the neat ABS and the PPy-treated one are nearly indistinguishable, with the latter being slightly stiffer and more brittle. As a result, in the remainder of this paper we will always use neat ABS properties to represent also PPy treated ABS, i.e., also at other infill density values. This justifies also the assumption of treating the PPy-treated ABS as a single material in the FEM simulations. On the other hand, the copper-plated ABS shows a remarkable improvement in the mechanical properties compared with the other materials, despite the copper layer is very thin (i.e., $\approx 100 \pm 0.01$ μm). This can be explained because copper is stronger and stiffer than ABS and since it is deposited far from the neutral axis of the specimen, it is very effective in increasing the flexural properties. Interestingly, the copper-plated specimens have a peculiar shape of the stress–strain curve, displaying three different slopes, the first one between 0 and 0.1%, the second one between 0.1% and 3%, and the last one at higher strains.

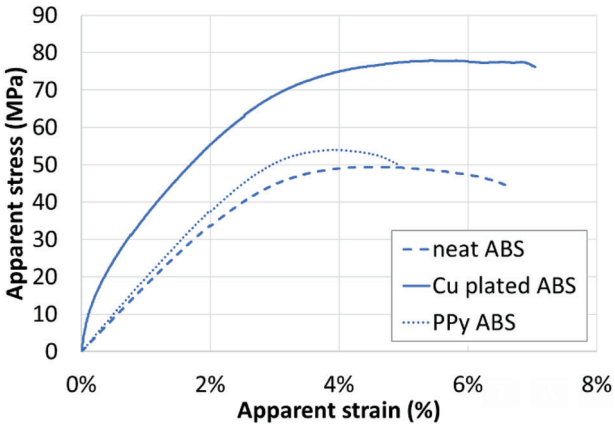

Figure 4. Stress versus strain curves of neat and coated ABS specimens with 100% infill density.

Table 2. Bending properties for all materials with 100% infill density.

Material	Stiffness [N mm^{-1}]	Apparent Young's Modulus [GPa]	Maximum load [N]	Apparent Strength [MPa]
Neat ABS	11.27 ± 0.46	1.80 ± 0.21	68.41 ± 1.0	50.1 ± 0.8
PPy treated ABS	12.24 ± 0.85	1.93 ± 0.34	67.81 ± 2.23	54.0 ± 1.54
Copper plated ABS	59.40 ± 7.82	6.69 ± 1.03	119.4 ± 1.65	78.75 ± 2.22

The Young's moduli of the various materials are proportional to the stiffness of the load–displacement curve through a geometry-related scale factor, according to Equation (3). Stiffnesses and Young's moduli are listed in **Table 2** for all 100% infill materials together with maximum load and apparent strength. In the case of the copper-plated material, the apparent Young's modulus was calculated using the first slope of the curve, i.e., the stiffest one.

To better understand the experimental measurements, the load versus displacement curve of the copper-plated specimens was compared to the same curve obtained by a finite element simulation of the bending test. The material parameters used for the FEM simulations are listed in **Table 3**. For the ABS core, the values of Young's modulus, yield strength, and hardening rule slope were taken from the curves of Figure 4, while the Poisson's ratio was assumed to be equal to 0.4. The copper layer properties were declared in Section 2.5.

The FEM simulations were first run with a 100 μm layer of copper all around the sample, assuming perfect adhesion between copper and ABS (**Figure 5a**). The results are shown in **Figure 6** and indicated as the "four-layer model" curve (i.e., the black curve). For ease of comparison, Figure 6 reports also the experimental load–displacement curve of the copper-plated material (blue curve), which is qualitatively the same as that of Figure 4, just differing by a scale factor. It can be clearly seen that the model overestimates the experimental results by a large amount.

On the other hand, it is quite evident that during the bending test, the upper copper layer detaches from the ABS substrate, as clearly shown in **Figure 7**. This can be easily explained through a buckling instability of the thin copper layer on the top surface, which is loaded in compression, together with a weak interfacial bond between plastic and metal. Moreover, also the copper layer on the lateral surface of the sample shows some amount of detachment (Figure 7).

To verify this, a different finite element simulation was performed. Assuming that the top copper layer did not contribute to carrying the applied load, the new simulation consisted of an incomplete copper plating, in that the top ABS surface remained clear of copper, while the copper plating on the lateral surface was

Table 3. Material parameters used for FEM simulations.

Material	Young's Modulus [GPa]	Yield stress [MPa]	Poisson Coefficient	Hardening rule slope [MPa]	Layer thickness [mm]
Copper	117	200	0.34	10 000	0.1
ABS 100%	1.80	45	0.4	50	4

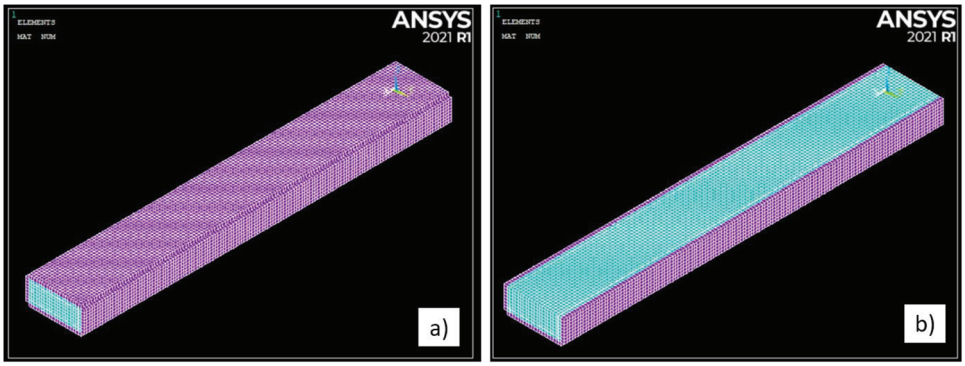

Figure 5. Geometry and mesh of a) four-layer model and b) three-layer model.

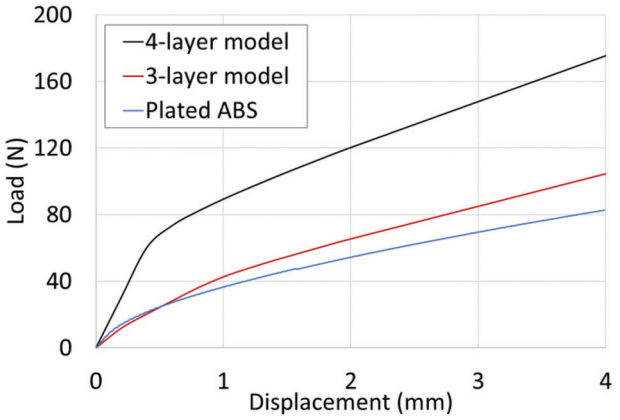

Figure 6. Load versus displacement curves of 100% infill density materials. Experimental plated ABS is in blue, four-layer model in black, and three-layer model in red. The black line overestimates the experimental data by a large amount, while the red line is much closer to the experimental data.

considered to yield at ≈50% of the nominal yield stress, in order to partially capture the damage in this portion of the specimen (Figure 5b). Copper, though, was still assumed to perfectly adhere to the polymeric substrate. The results of this simulation are displayed in Figure 6 as the curve labeled "three-layer model", which indeed is much closer to the experimental one, thus providing validation to the hypothesis that the top layer detaches from the specimen: the specimen behaves as if only the bottom copper layer is present.

At this juncture, it is convenient to discuss about the failure mechanism of the specimen. Despite failure appears at first glance to occur at the interface between copper and polymer, a closer look reveals something different. If one carefully peels off the copper layer from the PPy-treated ABS substrate of a pristine specimen, as pictured in **Figure 8**, the black PPy can be seen both on top of the ABS and underneath the copper layer. This shows that the adhesion of PPy is of rather good quality both on ABS and copper. Failure is then a cohesive failure of the thin PPy coating that has been directly polymerized on the ABS substrate. This is reasonable, because PPy polymerizarion following the protocol described in Section 2.2 most likely results in a low molecular weight polymer, thus possessing low strength. In any case, what appeared to be an interface failure, is actually the cohesive failure of the electrically conductive polymeric layer.

The mechanical behavior of the 100% infill density copper-plated specimen, with its three-slope shape of the load–displacement curve (Figure 4) can then be explained through the following chain of events. Initially, the specimen is intact,

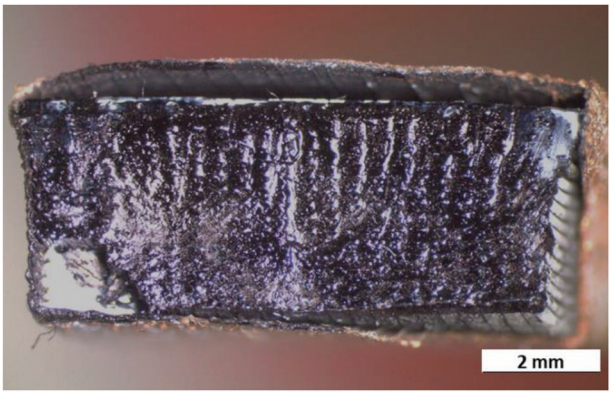

Figure 7. Fracture surface of 100% infill density of copper-coated specimen. The upper part is loaded in compression, thus it buckles and detaches from the ABS substrate.

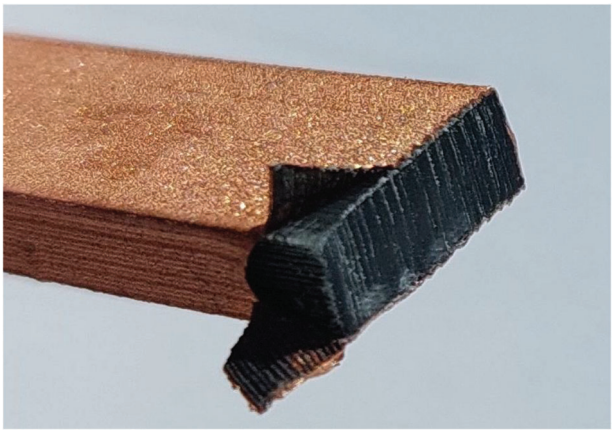

Figure 8. Peeling off of the copper plating from the ABS substrate, revealing the cohesive failure of the thin PPy layer.

Table 4. Average mass and apparent density of the neat and plated ABS samples as a function of the infill density. For each infill, the mass of deposited copper is indicated.

Infill [%]	Average mass [g]			Apparent density [g cm^{-3}]	
	Neat ABS	Plated ABS	Deposited copper	Neat ABS	Plated ABS
30	1.26 ± 0.01	9.97 ± 0.22	8.71 ± 0.20	0.39	2.90
40	1.58 ± 0.01	11.59 ± 0.20	10.01 ± 0.18	0.49	3.17
50	1.89 ± 0.01	12.15 ± 0.03	10.26 ± 0.04	0.59	3.20
60	2.19 ± 0.01	12.42 ± 0.01	10.23 ± 0.01	0.68	3.23
70	2.50 ± 0.02	13.08 ± 0.30	10.58 ± 0.30	0.78	3.25

thus its behavior can be well represented by the four-layer model of Figure 5. In fact, the initial part of the experimental load–displacement curve of Figure 6 (the blue one) is rather stiff, quite close to the black curve representing the four-layer model. After reaching ≈0.1% strain, though, the top copper layer undergoes compressive instability, it buckles and detaches from the ABS substrate, due to the cohesive failure of the PPy between copper and ABS. The specimen thus becomes more similar to the three-layer model of Figure 5, and consequently, the blue curve of Figure 6 (the experimental one) becomes more similar to the red one representing the three-layer model. The next step is the yielding of the bottom copper layer, which is very clear in the red curve of Figure 6, but can also be in the experimental blue curve. Finally, also the PPy treated ABS yields, and this can be clearly seen in Figure 4, at ≈3% strain.

It is quite clear that specimen failure starts because of the poor quality of the PPy. An improvement can be sought by increasing the total extension of the interface, thereby reducing the net stress on the PPy and making it more difficult to detach the metal plating from the polymeric substrate. To this goal, the infill density was varied, so that the open porosity that is created on the printed ABS surface could allow the penetration of the electrodeposited copper, promoting mechanical interlocking with the PPy-treated ABS substrate.

In **Table 4**, the average mass and the apparent density of the neat and plated ABS samples as a function of the infill density are listed. The mass of the deposited copper is reported in Table 4 as the difference between that of neat ABS prior to electroplating and the mass of the copper-plated specimen, neglecting the mass of the PPy coating. Notice that the mass of the deposited copper was held about constant for each infill density, except for the lowest one, and was chosen in such a way as to maintain in all cases the apparent density of the final specimen comparable with a lightweight alloy (i.e, ≈3 g cm^{-3}).

In **Figure 9** the upper surface of the specimens at various infill densities is displayed. The pictures show that the copper layer is well-deposited for all infill density values. For infill densities up to 50%, the metal is deposited on the extruded beads leaving the specimen with an open porosity that is exposed on the surface, while at higher infill values the copper coating seems to fill the voids so that the surface appears clear of porosity.

This is confirmed by looking at **Figure 10**, where the cross sections of the bending samples at various infill densities are displayed. At 70% and 60% infill densities, the copper plating penetrates partially into the sample from the outer surfaces toward the center, but seemingly without crossing it completely. As the infill density decreases below 50%, copper is deposited also in the interior of the sample down to its core, covering the internal surfaces completely, thereby creating through-thickness bridges between the outer layers.

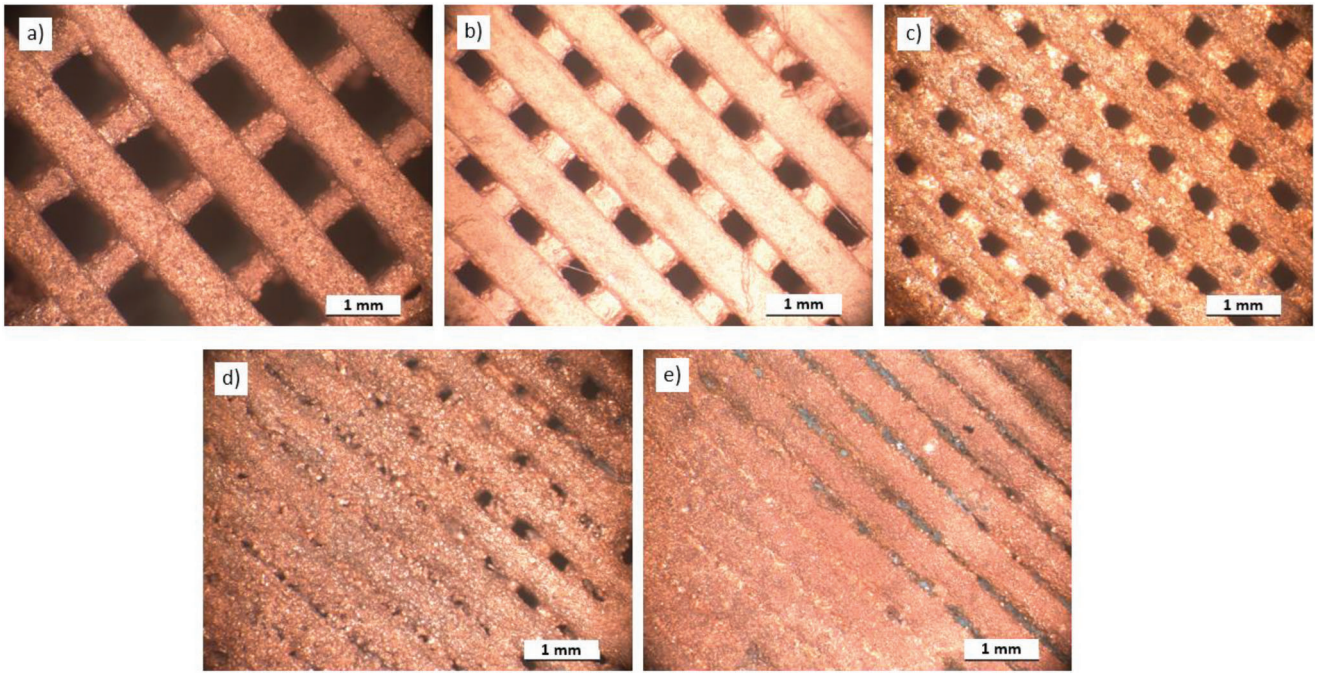

Figure 9. Surface morphology by optical microscope of a) 30%, b) 40%, c) 50%, d) 60%, and e) 70% infill density of copper-coated specimens.

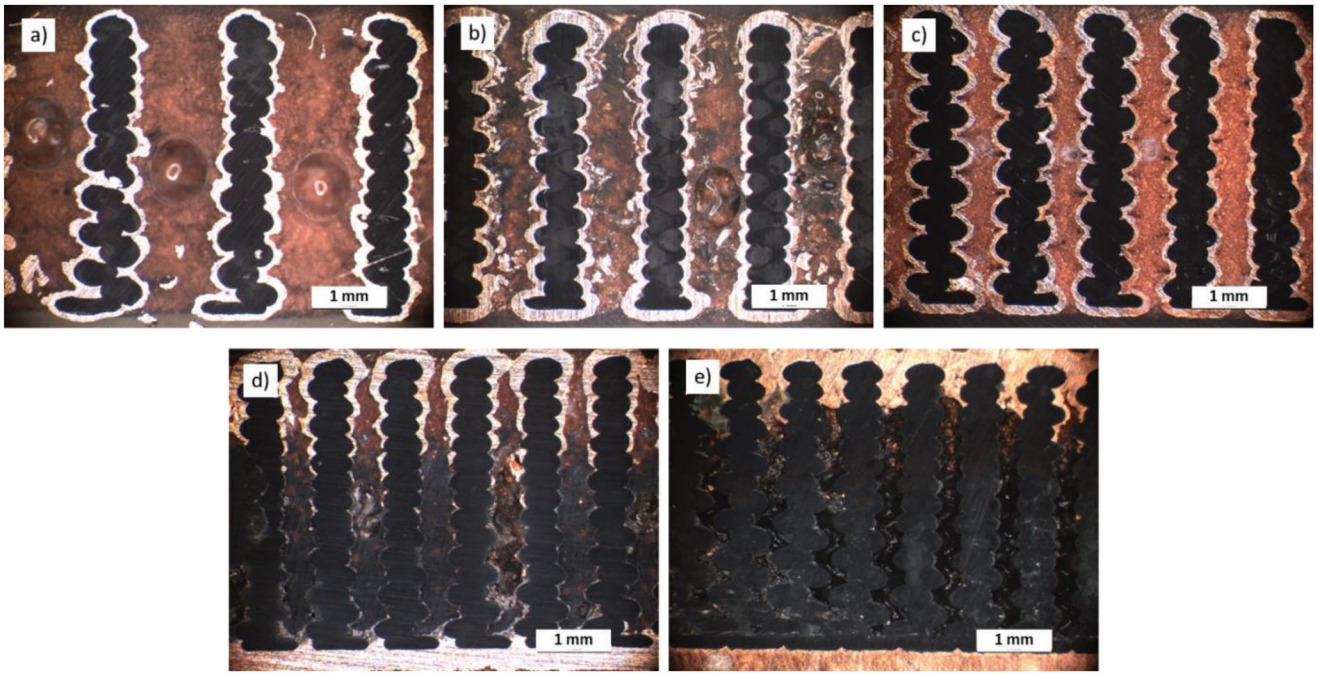

Figure 10. Cross section of flexural specimens of a) 30%, b) 40%, c) 50%, d) 60%, and e) 70% infill density of copper plated specimens.

In **Figure 11**, the apparent stress versus strain curves of the neat and plated ABS at various infill densities, are shown. As expected, for neat ABS both apparent flexural strength and strain at break decrease with the infill density, since the amount of material decreases. Observing the plated ABS curves, the apparent flexural strength follows a similar behavior, although at higher infill percentages the differences between the compositions are less discernible.

Comparing the curves of neat (Figure 11a) and copper-plated ABS (Figure 11b), it is clear that the presence of the outer metal layer is effective in producing a remarkable increase in the flexural strength. On the other hand, the copper-plated ABS curves with higher values of infill densities (i.e., 60% and 70%) (Figure 11b) show a significant strength increase if compared to that at 100% infill density (Figure 4). On the other hand, the presence of the metal plating produces a certain decrease in the deformation at break.

In **Table 5**, the mean and standard deviation of the apparent Young's modulus and strength for neat and plated ABS are listed. Also in this case, the apparent stiffness of the neat ABS decreases as a function of the infill density, while for the plated ABS, the apparent Young's modulus shows a maximum peak for the 60% infill density material, but the value for the 70% infill density material is not significantly different. On the other hand, apparent strength values are always increasing with infill density.

The flexural properties that were obtained demonstrate that a relatively small decrease in the infill density produces a significant improvement in total strength, due to a better mechanical bond between the substrate and the metal layer. On the other hand, the flexural properties decrease when the infill density is <50%, and this is essentially due to the fact that copper penetrates to the interior of the specimen, closer to the neutral axis, thus it is ineffective in reinforcing the material in bending.

As for the 100% infill density, the load versus displacement curves of the 60% and 70% infill density copper plated ABS were compared with the corresponding finite element simulations, and this is shown in **Figure 12**. The material parameters that were used for the FEM simulations are listed in **Table 6**, considering

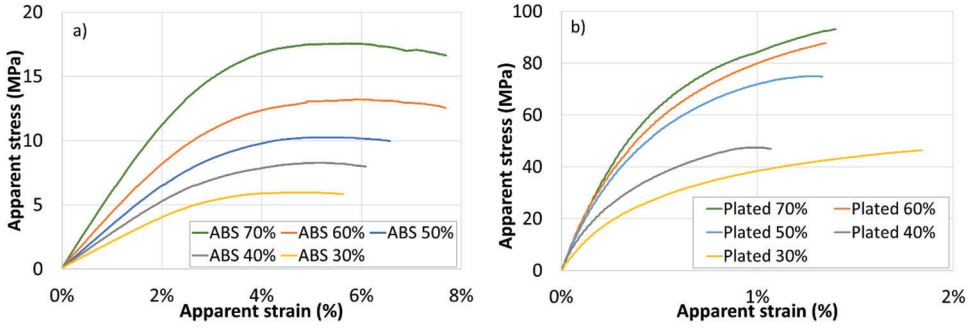

Figure 11. Apparent stress–strain curves of a) neat ABS and b) plated ABS at various infill densities.

Table 5. Bending properties as a function of the infill density for neat and plated ABS.

	Infill [%]	Stiffness [N mm^{-1}]	Apparent Young's Modulus [GPa]	Maximum Load [N]	Apparent Strength [MPa]
Neat ABS	30	1.47 ± 0.04	0.21 ± 0.01	8.96 ± 0.16	6.09 ± 0.14
	40	1.90 ± 0.01	0.27 ± 0.01	11.75 ± 0.23	8.09 ± 0.15
	50	2.33 ± 0.02	0.34 ± 0.02	15.03 ± 0.13	10.28 ± 0.04
	60	3.07 ± 0.04	0.43 ± 0.03	19.60 ± 0.21	13.43 ± 0.19
	70	4.22 ± 0.09	0.60 ± 0.05	25.75 ± 0.44	17.68 ± 0.41
Plated ABS	30	93.04 ± 3.71	9.5 ± 0.13	79.13 ± 12.16	43.41 ± 3.70
	40	107.61 ± 15.09	14.9 ± 2.27	94.11 ± 16.41	44.78 ± 3.76
	50	143.19 ± 10.57	17.2 ± 1.98	126.09 ± 9.89	71.33 ± 3.33
	60	207.30 ± 9.98	21.9 ± 1.54	178.98 ± 15.79	85.78 ± 2.38
	70	224.61 ± 3.39	19.3 ± 0.15	204.66 ± 13.06	96.82 ± 3.47

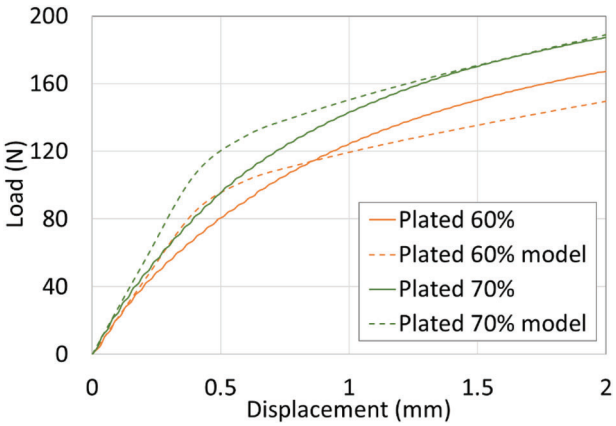

Figure 12. Load versus displacement curves of plated ABS with 60% and 70% infill densities compared with corresponding FEM models.

that the material properties of copper are the same as those used previously (Table 3).

The simulations were performed only for the two infill densities that showed the highest flexural properties, i.e., 60% and 70%. The experimental curve of the plated ABS with 70% infill density is very close to the one modeled by FEM simulation, both in terms of apparent Young's modulus and flexural strength.

This result confirms that copper plating exploits the surface porosity created by the infill decrease to penetrate inside the sample and create an effective bond with the polymeric substrate. Thus, mechanical interlocking allows to obtain mechanical properties that are virtually identical to those of a perfect interface, as supposed in the FEM model. On the other hand, the numerical model for the plated ABS with 60% infill density shows a good estimate of the stiffness, while it slightly underestimates the flexural strength. This can be explained because in the 60% infill density sample, part of the deposited copper penetrated deeper into the sample (Figure 9d), and this was neglected in the FEM simulation.

It must be pointed out that the difference in qualitative behavior between the experimental results and the FEM simulations comes from the elasto-plastic model that was implemented in the FEM simulation, which does not correspond to the real material behavior, especially in the case of the modeling of the polymeric core, which is not elasto-plastic, but rather follows a non-linear viscoelastic behavior. On the other hand, the goal of these FEM simulations was not to model the mechanical behavior precisely, but only to understand the effectiveness of copper plating in enhancing the mechanical properties of the final material.

3.2. Thermal Properties

Concerning the effect of PPy treatment, the apparent thermal diffusivity at 100% infill of neat ABS is very close to that of PPy-treated ABS (0.108 ± 0.005 and 0.112 ± 0.004 mm^2 s^{-1}, respectively). These values are much less than those of copper-plated specimens, which are pictured in **Figure 13** as a function of the infill density, thus it is clear that the copper plating crossing the sample thickness leads to a remarkable improvement in the apparent thermal diffusivity.

More in detail, the apparent diffusivity increases with the infill density percentage, until it reaches a maximum value at 50% and then decreases. This value probably maximizes the number of effective highly conductive copper bridges crossing the whole specimen thickness: at lower infill percentages there are fewer copper bridges traversing the specimen thickness (Figure 10a,b compared with Figure 10c), while at higher infill densities, even if more bridges could be there, only some of them (Figure 10d)

Table 6. Material parameters used for FEM simulations.

Material	Apparent Young's Modulus [GPa]	Yield stress [MPa]	Poisson Coefficient	Hardening rule slope [MPa]	Copper thickness [mm]
ABS 60%	0.43	12	0.4	40	0.15
ABS 70%	0.60	16	0.4	50	0.2

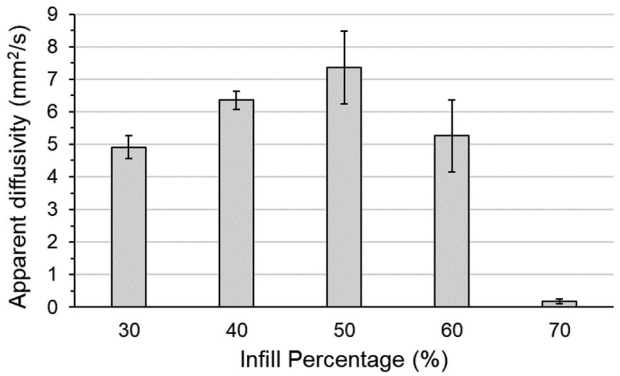

Figure 13. Apparent diffusivity as a function of the infill density.

or even none of them (Figure 10e) are able to cross the whole specimen, thus they may be partly ineffective.

4. Conclusion

This study investigated the effect of a two-step copper electrodeposition process on the mechanical and thermal properties of FFF 3D printed ABS parts, at different infill densities. A thin copper layer over the surface of 3D printed parts with 100% infill density increases the flexural properties only slightly. It was found that this is due to the cohesive failure of the PPy layer that is necessary to increase the electrical conductivity of the ABS substrate prior to electroplating.

On the other hand, if the infill density is decreased, the electrodeposited copper is able to partly penetrate through the sample surface, creating an effective mechanical interlocking with the polymer, thus decreasing the net loading on the PPy coating and enhancing the metal-polymer interface strength. As a result, this produces a significant improvement in the flexural properties for infill density values in the 60–70% range, both in terms of apparent Young's modulus and apparent strength. This idea can be also exploited by modulating the surface roughness of 3D printed objects, for example by texturing, in such a way to increase the external surface area and thus the interfacial adhesion.

Moreover, copper deposition over ABS parts led also to an interesting improvement in thermal diffusivity. In particular, this occurred mainly for an infill density of 50% or lower, because the through-thickness copper penetration allows the creation of thermo-conductive bridges that enhance thermal properties.

Combining all of the above, if a certain application of a 3D printed copper electroplated part requires adequate thermal and mechanical properties simultaneously, the best compromise is to maintain an infill density value between 50% and 60%, as copper would mainly be deposited away from the neutral axis, thus enhancing the flexural properties, but many thermally conductive bridges would be created through the thickness of the part in such a way to insure adequate thermal conductivity.

Conflict of Interest

The authors declare no conflict of interest.

Data Availability Statement

The data that support the findings of this study are available from the corresponding author upon reasonable request.

Keywords

electroplating, flexural properties, fused deposition modeling, material extrusion, thermal diffusivity

Received: June 5, 2023
Revised: July 19, 2023
Published online: August 27, 2023

[1] S. Vyavahare, S. Teraiya, D. Panghal, S. Kumar, *Rapid Prototyp. J.* **2020**, *26*, 176.
[2] P. K. Penumakala, J. Santo, A. Thomas, *Compos. B. Eng.* **2020**, *201*, 108336.
[3] M. J. Kim, M. A. Cruz, S. Ye, A. L. Gray, G. L. Smith, N. Lazarus, C. J. Walker, H. H. Sigmarsson, B. J. Wiley, *Addit. Manuf.* **2019**, *27*, 318.
[4] L. Malagutti, V. Mazzanti, F. Mollica, *Rapid Prototyp. J.* **2022**, *28*, 1834.
[5] M. Sugavaneswaran, P. Thomas, A. Azad, *FME Trans* **2019**, *47*, 880.
[6] C. Eßbach, D. Fischer, D. Nickel, *J. Manuf. Process.* **2021**, *68*, 1378.
[7] S. Wickramasinghe, T. Do, P. Tran, *Polymers* **2020**, *12*, 1529.
[8] A. A. Bakir, R. Atik, S. Özerinç, *Rapid Prototyp. J.* **2021**, *27*, 537.
[9] V. Mazzanti, L. Malagutti, F. Mollica, *Polymers* **2019**, *11*, 1094.
[10] L. Malagutti, G. Ronconi, M. Zanelli, F. Mollica, V. Mazzanti, *Processes* **2022**, *10*, 2399.
[11] L. Malagutti, V. Mazzanti, F. Mollica, *Rapid Protyp. J.* **2022**, *28*, 1834.
[12] L. Malagutti, S. Charlon, V. Mazzanti, F. Mollica, *J. Mater. Proc. Tech.* **2023**, *316*, 117961.
[13] S. Olivera, H. B. Muralidhara, K. Venkatesh, K. Gopalakrishna, C. S. Vivek, *J. Mater. Sci.* **2016**, *51*, 3657.
[14] R. Melentiev, A. Yudhanto, R. Tao, T. Vuchkov, G. Lubineau, *Mater. Des.* **2022**, *221*, 110958.
[15] A. Equbal, M. I. Equbal, A. K. Sood, M. A. Equbal, *J. Technol.* **2017**, *8*, 930.
[16] M. S. N. M. Shaikh, B. B. Ahuja, *Mater. Today: Proc.* **2020**, *41*, 875.
[17] U. A. Danade, S. D. Londhe, R. M. Metkar, *Rapid Prototyp. J.* **2019**, *25*, 1224.
[18] P. K. Gurrala, B. Tripathi, *Key Eng. Mater.* **2019**, *821*, 137.
[19] A. K. Sood, A. Equbal, *Mater. Today: Proc.* **2020**, *28*, 1154.
[20] M. Bazzaoui, J. I. Martins, E. A. Bazzaoui, A. Albourine, R. Wang, P.o-D.a. Hong, *Surf. Coat.* **2013**, *224*, 71.
[21] V. Srisupornwichai, C. Aumnate, P. Visuttipitukul, S. T. Dubas, M. Metzner, M. Zinn, Y. Boonyongmaneerat, *Curr. Appl. Sci.* **2022**, *22*, 10.
[22] S. K. Padhi, S. S. Mahapatra, R. Padhi, H. C. Das, *Adv. Manuf.* **2018**, *6*, 442.
[23] M. S. Khan, S. B. Mishra, M. A. Kumar, D. Banerjee, *Mater. Today: Proc.* **2018**, *5*, 19011.
[24] T. Maciag, J. Wieczorek, W. Kalsa, *Arch. Metall. Mater.* **2019**, *64*, 639.
[25] E. Vanecková, M. Bousa, R. Sokolová, P. Moreno-García, P. Broekmann, V. Shestivska, J. Rathouský, M. Gál, T. Sebechlebská, V. Kolivoska, *J. Electroanal. Chem.* **2020**, *858*, 113763.
[26] K. Angel, H. H. Tsang, S. S. Bedair, G. L. Smith, N. Lazarus, *Addit. Manuf.* **2018**, *20*, 164.
[27] T.'. V. Vernitskaya, O. N. Efimov, *Russ. Chem. Rev.* **1997**, *66*, 443.
[28] J. Nemati, G. H. Majzoobi, S. Sulaiman, B. T. H. T. Baharudin, M. A. Azmah Hanim, *Int. J. Miner.* **2014**, *21*, 569.
[29] S. Zhang, M. Sakane, T. Nagasawa, K. Kobayashi, *Procedia Eng.* **2011**, *10*, 1497.

